

Eclipsing binary search in the QUEST low latitude catalogue and the ELLISA light curve simulator

Bolivia Cuevas-Otahola^{1,2,3}, Cecilia Mateu^{1,4}, Fabiola Hernández-Pérez²,
Juan José Downes^{1,5}, A. Katherina Vivas⁶ and César Briceño⁶

¹*Centro de Investigaciones de Astronomía, AP 264, Mérida 5101-A, Venezuela*

²*Universidad de Los Andes, Facultad de Ciencias, Departamento de Física, Mérida, Venezuela*

³*Instituto Nacional de Astrofísica, Óptica y Electrónica, Ap. 51, 72000 Puebla, México, México*

⁴*Departamento de Astronomía, Instituto de Física, Universidad de la República, Igúá 4225, 11400 Montevideo, Uruguay*

⁵*PDU Ciencias Físicas, Centro Universitario Regional del Este (CURE), Universidad de la República, 27000 Rocha, Uruguay*

⁶*Cerro Tololo Inter-American Observatory, National Optical Astronomy Observatory, Casilla 603, La Serena, 1700000, Chile*

Released 2019 Xxxxx XX

ABSTRACT

The realistic simulation of variable star populations is fundamental to determine the selection function and contamination in existing and upcoming multi-epoch surveys. We present ELLISA, a simulator that produces an ensemble of mock light curves for a population of eclipsing binaries obtained from physical and orbital parameters consistent with different galactic populations, and which considers user-supplied time sampling and photometric errors to represent any given survey. We carried out a search for eclipsing binaries in the QUEST low-galactic latitude catalogue of variable stars, spanning an area of 476 sq. deg at $-25^\circ \lesssim b \lesssim 30^\circ$ and $190^\circ \leq l \leq 230^\circ$ towards the galactic anti-centre, and use ELLISA to characterise the completeness of the resulting catalogue in terms of amplitudes and periods of variation as well as eclipsing binary type. The resulting catalogue consists of 1,125 eclipsing binaries, out of which 179, 60 and 886 are EA, EB and EW types respectively. We estimate, on average, 30% completeness in the period range $0.25 \lesssim P/d \lesssim 1$ for EB+EW binaries and 15% completeness for EA binaries with periods $2 \lesssim P/d \lesssim 10$, being the time sampling the primary factor determining the completeness of each type of eclipsing binary. This is one of few eclipsing binary catalogues reported with an estimate of the selection function. Mock eclipsing binary light curve libraries produced with ELLISA can be used to estimate the selection function and optimise eclipsing binary searches in upcoming multi-epoch surveys such as Gaia, the Panoramic Survey Telescope and Rapid Response System, the Zwicky Transient Factory or the Large Synoptic Survey Telescope.

Key words: (stars:) binaries: eclipsing, astronomical data bases: catalogues, methods: numerical

1 INTRODUCTION

Eclipsing binaries are widely recognised for their importance in different astrophysical areas. In variability surveys, they are usually the most abundant type of variable star, particularly at low Galactic latitude. Although the specific proportions depend on each survey's depth, cadence and area probed (particularly galactic latitude), in the All Sky Automated Survey (ASAS, [Pojmanski 1997](#)) and Catalina Real-Time Transient Survey ([Drake et al. 2014a](#), CRTS,) they amount to 25% and 58% percent of all variable stars respectively.

Eclipsing contact binaries or W-UMa type variables

(EWs), in particular, follow a Period-Luminosity-Colour relation ([Rucinski 1994](#); [Rucinski & Duerbeck 1997](#)), which implies they can serve as standard candles for distance measurements ([Rucinski 1996](#)). The latest estimates give an error of ± 0.25 mag in distance modulus for these stars, which corresponds to a distance uncertainty of $\sim 12\%$ ([Rucinski 2004](#)). Although significantly fainter ($M_V > 2$) than other, more traditional, standard candles such as RR Lyraes ($M_V \sim +0.6$) and Cepheids ($M_V < -2$), EWs are numerous and ubiquitous as they trace populations of any age and metallicity. The advent of deep all-sky multi-epoch surveys such as Gaia, the Panoramic Survey Telescope and Rapid Response System (PanSTARRS), the Zwicky Transient Fac-

tory (ZTF) or the Large Synoptic Survey Telescope (LSST) (Gaia Collaboration et al. 2017; Kaiser et al. 2010; Ivezić 2010; Smith et al. 2014), together with the first 3D extinction maps (Sale et al. 2014; Green et al. 2015), will open up the opportunity to use EWs as tracers of Galactic structure for the first time. For example, Gaia will be capable of observing an $M_V = 3$ EW star up to ~ 30 kpc without extinction, or up to ~ 15 kpc with $A_V = 1$, effectively probing a considerable volume of the Galactic Disc and inner Halo.

Numerous works have shown many potential uses for standard candles as probes of Galactic structure, e.g. to discover and trace stellar overdensities, clouds and tidal streams (e.g. Vivas & Zinn 2006; Sesar et al. 2010b; Baker & Willman 2015), trace radial and vertical metallicity gradients (Luck et al. 2006) and to measure the density profiles of different Galactic components (e.g. Brown et al. 2008; Vivas & Zinn 2006; Sesar et al. 2010a; Cohen et al. 2017). However, for any tracer catalogue to be useful for studies of the Galactic density profiles, a thorough understanding of its completeness is required, which needs to be estimated through simulations. In RR Lyrae surveys, light curve simulations have been done extensively to model the survey completeness. Vivas et al. (2004); Miceli et al. (2008); Mateu et al. (2012, hereafter M12); Sesar et al. (2017), for example, produce synthetic light curve catalogues for a population of mock RR Lyrae stars, which are then run through the period-finding and RR Lyrae identification algorithms used to characterise the survey’s completeness by looking at the fraction of recovered stars as a function of different parameters, such as magnitude, amplitude and number of observations. This completeness in the identification of RR Lyrae stars can range from $\sim 60\%$ in the SEKBO and Catalina surveys (Keller et al. 2008; Drake et al. 2013; Torrealba et al. 2015) to as high as $> 90\%$ in LONEOS, SDSS Stripe 82, PS1 or QUEST (Sesar et al. 2010b, 2017; Vivas et al. 2004, M12). Estimates such as these, however, have not been provided to date for eclipsing binary surveys.

The fact that eclipsing binaries are the most common type of variable star also means they are a very common contaminant in surveys for other types of variables. EWs are frequent contaminants of RRc and Delta Scuti surveys (e.g. Vivas et al. 2004; Kinman & Brown 2010, M12). Their light curve period ranges are similar (from a few hours to $\lesssim 1.5$ d), and when time sampling is irregular and observations sparse, the light curve shapes can be difficult to tell apart and period aliasing can be a source of confusion.

Although currently many codes exist to simulate eclipsing binary light curves, such as NightFall (Wichmann 2011), Wilson-Devinney (WD, Wilson & Devinney 1971) and EBOP (Eclipsing Binary Orbit Program, Etzel 1981), these are oriented towards simulating light curves for individual binary systems in great detail. However, as a population, eclipsing binary light curves are difficult to model because stars in almost any two evolutionary stages can be part of a binary system and the proportions of the different types of stars paired have to be modelled consistently with the initial mass function and star formation history of the population, and the effects of mass transfer on the stellar evolution of each component (see e.g. Hernández-Pérez & Bruzual 2013). Prša et al. (2011) approached this problem to estimate the eclipsing binary yield of LSST by simulating a library of eclipsing binary light curves with physical and orbital pa-

rameters drawn at random from a set of given distributions, which were then fed into PHOEBE (Prša & Zwitter 2005), a code based on WD.

Our goal in this work was, therefore, to develop a tool to simulate light curves for populations of eclipsing binaries. ELLISA (Eclipsing binary Light curve LIBrary SimulAtoR), is based on stellar population synthesis models (Hernández-Pérez & Bruzual 2013) to produce binary systems with physical characteristics and in numbers consistent with the parent stellar population, and reproducing the observational characteristics of a given survey: time sampling, typical photometric errors in each filter, bright and faint magnitude limits, and so on (Section 2). The light curve catalogues simulated with ELLISA will allow characterizing the completeness and possible biases of any eclipsing binary search, serve as benchmarks for the optimization of eclipsing binary observing strategies and search algorithms, and provide estimates of the expected levels of contamination of searches for other types of variable stars. Finally, we use the QUEST low latitude catalogue of variable stars (M12) as a case study, and implement ELLISA to guide the search and characterise the completeness of the resulting eclipsing binary catalogue. The ELLISA code is publicly available at a GitHub repository¹.

This paper is organized as follows: Section 2 describes the ELLISA code, which is used to generate a mock catalogue to guide the search for eclipsing binaries in the QUEST catalogue of variable stars described in Section 3. Using the ELLISA mock catalogue, the completeness of the catalogue obtained is characterised in Section 4 as a function of amplitude, magnitude and spatial distribution, for each eclipsing binary type. Section 5 contains summary and conclusions.

2 ELLISA: ECLIPSING BINARY LIGHT CURVE LIBRARY SIMULATOR

The goal of the ELLISA simulator is to generate a library of synthetic multi-filter light curves for a population of eclipsing binaries, reproducing the time sampling and photometric errors representative of the survey the user wants to simulate. This makes it possible to generate a synthetic library that mimics the way we would observe a population of eclipsing binaries with an arbitrary instrument and time sampling. ELLISA is made publicly available as a Python stand-alone code and library at a GitHub repository¹.

The code’s structure is shown in Figure 1, where user inputs are shown with squares, subroutines used by ELLISA are shown in circles and the outputs produced are shown with rhombuses. The overall process is as follows. The user supplies ELLISA the stellar population type, filter set and number of binary systems to simulate. This data is used by a routine that works as a wrapper for the binary stellar population synthesis code HB13 by Hernández-Pérez & Bruzual (2013), which simulates a synthetic population of binary systems at zero-age of a simple stellar population (SSP), calculates its stellar evolution according to the selected initial mass function, and returns the physical pa-

¹ <https://github.com/umbramortem/ELLISA>

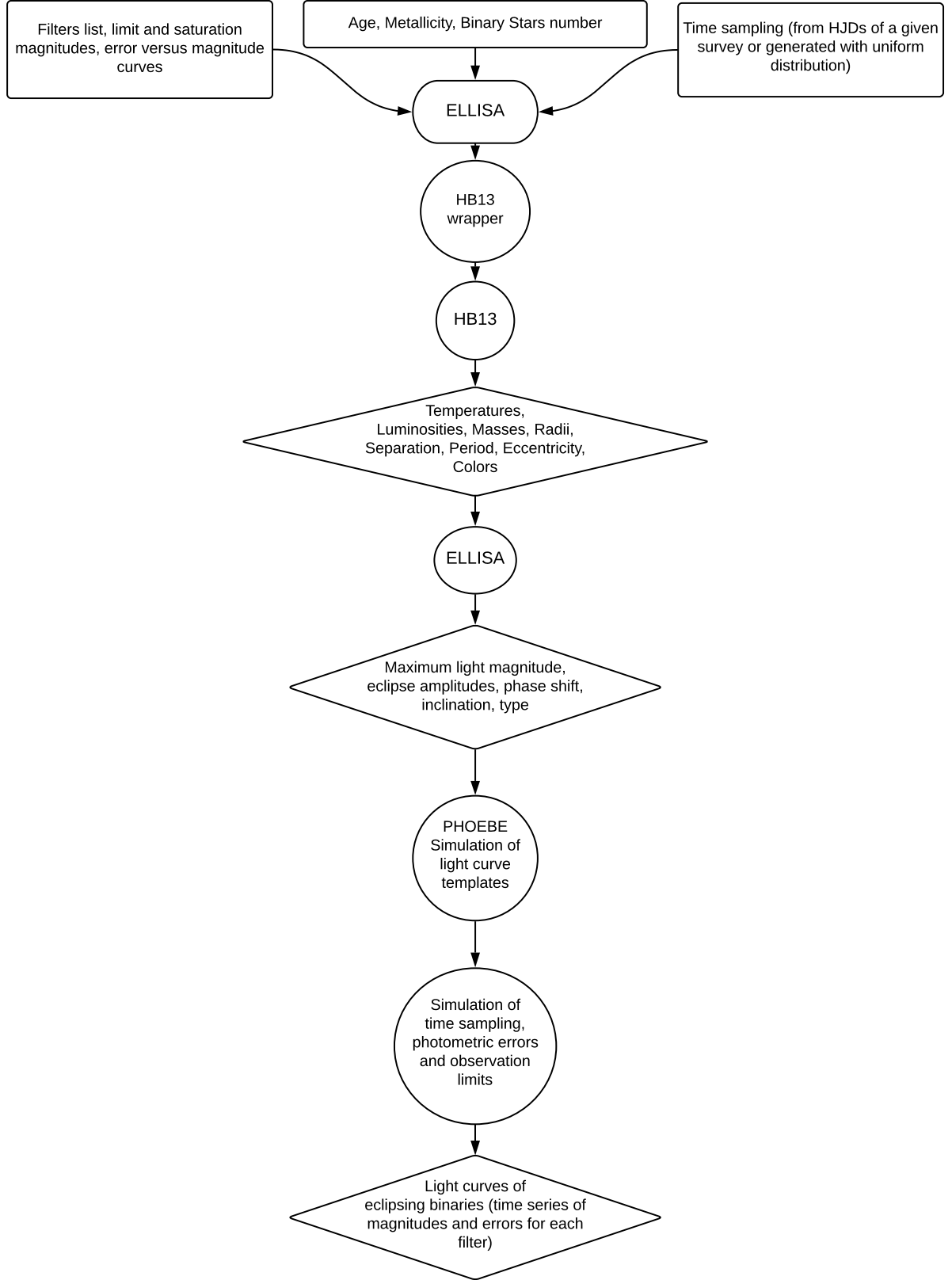


Figure 1. ELLISA flowchart. Rectangles, ellipses/circles and diamonds indicate user-supplied input, subroutines and outputs respectively.

rameters, magnitudes and colours of the individual stars in the binary population.

From these parameters the type of eclipsing binary (EW, EB and EA) is identified and, for each filter, light curve parameters –eclipse amplitudes, colours, maximum light magnitudes– are computed using the widely known code PHOEBE (Prša & Zwitter 2005). Then the observation process is simulated by sampling the light curve in the specific epochs given in the input time sampling, and the photometric errors and observation limits are simulated based on the (user-supplied) survey characteristics. Finally, the simulator returns the time series containing the magnitudes, photometric errors and observation dates for each binary system, in each filter selected by the user. In what follows we describe in detail each of these steps.

2.1 Simulation of Physical Parameters of Binaries using HB13

In this part, ELLISA uses the HB13 code from (Hernández-Pérez & Bruzual 2013) to generate the physical and orbital parameters –masses, separations, effective temperature, etc. – of the binary population, consistently with the stellar evolution of the population being simulated.

HB13 is a code developed by Hernández-Pérez & Bruzual (2013) that generates and follows the stellar evolution of an SSP, consisting of isolated stars and binary systems. This is implemented as a **Fortran** code, bundled and run inside ELLISA through a **Python** wrapper subroutine. Here we summarise the procedures followed by HB13, and we refer the reader to Hernández-Pérez & Bruzual (2013) for further details.

Stellar population selection The wrapper subroutine allows simulating predefined simple and composite stellar populations. In its current version, ELLISA allows the user to choose one of the following options, tailored to resemble the main Galactic components: Halo type, Bulge type, Thick disc type, Thin disc type.

The ages and metallicities used for the preset populations were chosen following (Robin et al. 2012, their Table 1). The Halo, Bulge and Thick Disc populations are simulated using SSPs, and the extended star formation history of the Thin Disc is simulated using 7 SSPs with ages between 100 Myr to 10 Gyr and metallicities between -0.12 dex and 0.01 dex, given by Robin et al. (2012). These SSPs are combined in equal proportions (by number) for each age bin, so as to approximately reproduce the star formation history of the Thin Disc with the local density reported by Robin et al. (2012) for each age bin.

Initial Physical and Orbital Parameters The physical and orbital parameters are simulated for the binary population at zero-age, as follows:

- Stellar masses (M_1) are randomly drawn from a Chabrier (2003) Initial Mass Function ranging from $0.1M_\odot$ to $100M_\odot$, parametrized as a log-normal distribution with characteristic mass $\log m_c = 0.08$ and variance $\sigma^2 = <(\log m - <\log m >)^2 > = 0.47$.
- For each potential primary star, a binary probability is drawn at random as a function of the spectral type, based

on the compilation by Lada (2006) summarized in Table 1. This reproduces the larger binary probability observed for more massive stars. It is important to stress that these correspond to binary fractions at zero age, which change as the stellar population evolves and the stellar evolution under the effects of mass transfer is taken into account. For example, the fraction of F-G primary stars in binaries changes from 13.7% at zero-age to 8.6% at 10 Gyr.

- For the stars randomly assigned to binary systems in the previous step, secondary masses are computed from a mass ratio q drawn at random from a uniform distribution ranging from 0 to 1. Reggiani et al. (2011) and Reggiani & Meyer (2013) find that distribution of mass ratios is consistent with being uniform ($dN/dq = q^{0.25 \pm 0.29}$) in the Galactic field, as well as in many star forming regions. They also find the mass ratio distribution to be independent of the binary separation.

- Orbital periods are drawn at random from the Duquennoy & Mayor (1991) log-normal distribution with mean $\log P(d) = 4.4$ and standard deviation $\sigma_{\log P} = 2.3$. Orbital semi-major axes are computed from Kepler’s Third Law $GMa^{-3} = 4\pi^2 P^{-2}$.

- Initial orbital eccentricities are randomly drawn from a uniform distribution ranging from 0 to 1.

Binary Evolution Having generated the orbital and physical parameters, the next step is to follow the stellar evolution of each binary system. HB13 uses the Hurley et al. (2002) evolutionary tracks in order to follow the evolution of each binary, taking into account the degree of mass transfer in each evolutionary stage, based on the stellar masses and radii, and the orbital parameters of the system. The evolutionary stages followed go from the zero-age main sequence to the remnant stages (black hole, neutron star or white dwarf) for stars with initial masses ranging from 0.1 to a $100 M_\odot$ and metallicities from $Z=0.0004$ to $Z=0.01$. In addition, to cover evolutionary aspects of He white dwarf stars with collisions considered by Hurley et al. (2002) as destroyed systems, Hernández-Pérez & Bruzual (2013) use the model proposed by Han et al. (2002) which assumes Extreme Horizontal Branch stars (EHB) are formed through this channel. The isochrones used in the model are built from the evolutionary tracks described in Hernández-Pérez & Bruzual (2013).

The Hurley et al. evolutionary tracks code allows computing the evolution of a binary system at any age, returning the temperature and luminosity for each star in the binary. Absolute magnitudes are computed using the BaSeL 3.1 (Westera et al. 2002) spectral library. Currently the photometric systems available are Johnson-Cousins (UBVR-I-JHK), SDSS (*ugriz*) and HST (F814W, F775W, F625W, F606W, F555W, F445W, F435W, F410W, F330W, F250W, F220W).

2.2 Calculation of light curve parameters using PHOEBE

Having generated the physical and orbital parameters for the binaries, ELLISA goes on to determine the light curve parameters (primary and secondary eclipse amplitudes, maximum light magnitude) corresponding to each system of the

Table 1. Binary fraction as function of spectral type

Spectral type	Binary fraction	Reference
O	0.72	Mason et al. 1998
O-B	0.65	Preibisch et al. 1999
B-A	0.62 ± 0.2	Patience et al. 2002
G-K	0.58 ± 0.1	Duquennoy & Mayor 1991
M	0.49 ± 0.09	Fischer & Marcy 1992
Late-type M	0.26 ± 0.1	Basri & Reiners 2006

simulated populations. The first step is to determine the light curve template to be used.

Light curves To generate the light curves we use PHOEBE (PHysics Of Eclipsing BinariEs) (Prša & Zwitter 2005), a modelling package for eclipsing binaries based on the well-known Wilson-Devinney code (WD, Wilson & Devinney 1971). We used the Legacy version of PHOEBE², with PYTHON implementation capabilities. We make use of the LC PHOEBE feature which employs the LC WD’s program to generate the light curve based on the binary’s physical and orbital parameters.

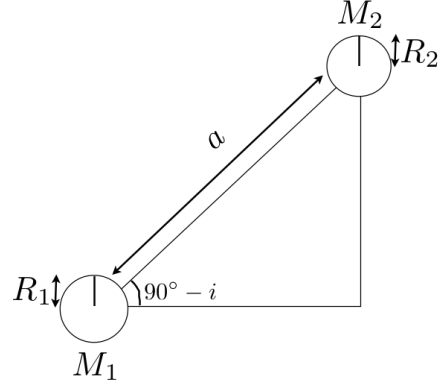
For this work we use the PHOEBE functionality for contact and detached systems. Therefore, two types of models are used to simulate the shapes of the eclipsing binary light curves: one for detached or Algol type, which hereinafter will be referred as EA systems, and another for semi-detached (β Lyrae) or contact (WUMa) systems, which in what follows will be referred as EB+EW systems (following the notation of the GCVS - General Catalog of Variable Stars Samus et al. 2009). The first step is to figure out whether the system is completely detached or not. For this, we follow Eggleton (2006) and for each binary we compute the critical period P_{crit} , i.e. the shortest period that a system with a certain mass ratio should have to make mass transfer events possible without overflowing its Roche lobe. According to Eggleton (2006) (their Eq. 3.10) the critical period is given by

$$P_{\text{crit}} \sim 0.35 \sqrt{\frac{R^3}{M_1}} \left(\frac{2}{1+q} \right)^{0.2}, \quad (1)$$

where M_1 and R denote the mass and radius of the primary and q the system’s mass ratio.

Through this criterion, we will separate the systems generated by HB13 into two blocks. The first group is constituted by EA systems whose separation is large enough to prevent mass transfer. A binary is of EA type if it has a period $P < P_{\text{crit}}$. The second, and complementary group, contains those systems with one or the two stars transferring mass to its companion, which correspond in this case to EB or EW light curves.

In order to shape the light curve on its entirety, given its type, the following orbital parameters are passed to PHOEBE to perform the orbit calculation:


Figure 2. Schematic representation of an eclipsing binary. Inclination-radius relation of the components.

- Initial inclination angle i of the orbital plane for each system, randomly drawn from a $\cos(i)$, $i \in [0, \pi]$ distribution (see e.g. Arenou 2011). The range of inclination angles in which a given binary will be detected as eclipsing is given by equation 2. This holds for EA, EW and EB systems. For shorter semi-major axes the range of inclination values is larger as we can see in Figure 2

$$a \cos(i) < R_1 + R_2. \quad (2)$$

- Eccentricity, period and semi-major axis distributions, given by HB13.
- Synchronicity parameter which is the ratio between rotation and orbital angular velocity, follows equation 3 when differential rotation is neglected

$$F = \sqrt{\frac{1+\epsilon}{(1-\epsilon)^3}}. \quad (3)$$

where ϵ is the orbital eccentricity.

- Argument of the periastron, randomly drawn from a uniform distribution in the range $[0, 2\pi]$

Once the orbit is added to the simulated system, the stellar parameters are also passed to PHOEBE in order to obtain geometrical light curves parameters.

Limb darkening effects are included in every system computation and are given as function of the selected passband in the case of the WD feature or can be dynamically computed from predefined tables (See PHOEBE scientific reference for further details).

The light curves physical quantities are given in units of flux, computed from the given passband luminosities in the available passbands systems (Stromgren, Johnson, Gaia, Tycho, Kepler, Hipparcos, LSST, Cousins).

Apparent magnitudes At this point we transform the absolute magnitudes to apparent ones by adding a distance modulus. For this, the user selects a reference band in which the final distribution of mean apparent magnitudes will be uniform and limited at the bright and faint ends by the user-supplied saturation and limiting magnitudes, respectively. The apparent magnitude in the reference band is drawn at

² <http://phoebe-project.org/1.0>

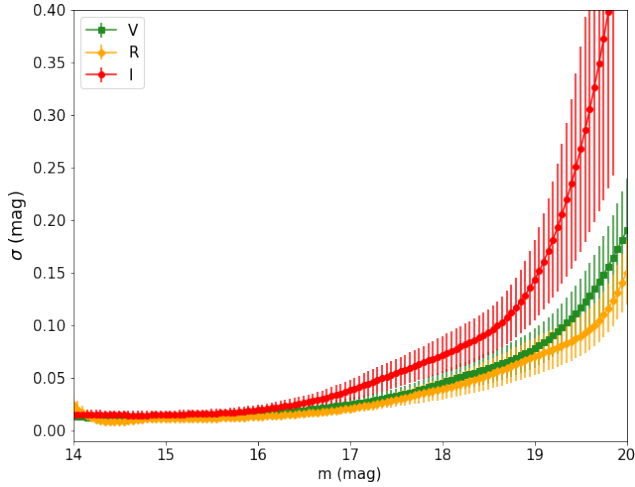


Figure 3. Error versus magnitude curves for QUEST catalogue in the VRI Johnson-Cousins filters, the bars represent the mean standard deviation δ of the typical photometric error σ at each magnitude.

random from this uniform distribution and the corresponding distance modulus is computed from the simulated absolute magnitude. This distance modulus is used to transform the magnitudes in the remaining bands from absolute to apparent. Finally, observations outside the (user-supplied) saturation and limiting magnitudes of each band are discarded.

2.3 Time sampling and photometric errors

The next step is to simulate the observation process, reproducing the time sampling, photometric errors and bright and faint limits of the survey for all the filters.

Time sampling The time sampling is generated by ELLISA based on user-supplied files containing the heliocentric julian dates (HJDs) of the observations in each filter.

The (error-free) magnitude m_i^{F0} is obtained by evaluating the light curve template for each filter F at the phase ϕ_i^F , corresponding to the t_i^F observation epoch, given by the following expression

$$\phi_i^F = \frac{t_i^F}{P} - \text{int}\left(\frac{t_i^F}{P}\right) + \phi_{\text{off}} \quad (4)$$

where t_i^F is the HJD of the i -th observation in the F filter, P is the light curve period and ϕ_{off} is the phase shift. The phase shift ϕ_{off} is randomly drawn from a uniform distribution in the range $\phi_{\text{off}} \in [0, 1)$. The phase-offset is filter-independent and it is taken as the phase in which the primary eclipse occurs.

Photometric errors The photometric errors are simulated as a function of magnitude, based on user-supplied error versus magnitude curves characteristic of the survey that is being simulated. As an example, Figure 3 shows error versus magnitude curves for the QUEST survey in the

VRI filters. These curves represent the mean standard deviation σ (in magnitudes) of non-variable stars per magnitude bin (Vivas et al. 2004, M12). The error bars are indicative of the actual dispersion of multiple measurements for non-variable stars at each magnitude bin, which we call δ , and represents the dispersion of the photometric error σ at that magnitude. The curves in Figure 3 were computed for the QUEST low-latitude catalogue of variable stars (M12).

The error-convolved magnitude is thus computed as $m_i = m_i^{F0} + \Delta m_i^F$, where Δm_i^F is a random number drawn from a gaussian distribution $G(0, \sigma)$ with zero-mean and standard deviation σ , which is, in turn, drawn from a gaussian $G(0, \delta)$ with zero-mean and standard deviation δ . Finally, error-convolved magnitudes outside the user-supplied bright and faint limits of the survey are discarded.

Figure 4 shows examples of synthetic light curves produced by ELLISA for eclipsing binaries of the three types: (upper panels) with periods of 0.4745 d (left) and 0.53 d (right), EB (middle panels) with periods of 0.6062 d (left) and 0.77 d (right) and EA (bottom panels) with periods of 3.2293 d (left) and 5.84 d (right), for the VRI filters. For each eclipsing binary type, two examples are shown to illustrate a very dense (>90) number of observations (left panels) and very sparse (~ 35) number of observations (right panels) time sampling characteristic of different areas of the QUEST M12 survey.

The ELLISA code takes approximately 40 minutes to run in an Intel Xeon(R) CPU E5-2620 v3 2.9GHz x24, to produce a light curve library for 1,000 eclipsing binaries.

2.4 Comparison of the ELLISA period distribution with Kepler

Here we compare the period distribution obtained by ELLISA with that from the Catalogue of Eclipsing Binaries (Kirk et al. 2016) from the Kepler mission. The Kepler catalogue was produced based on the very high number of observations of the Kepler mission, acquired during a long baseline, so it is a very homogeneous and complete survey of eclipsing binaries and is not expected to be significantly affected by observational biases, making a good reference for comparison.

Figure 5 shows the period distribution for an ELLISA simulation of eclipsing binaries in a Thin Disc population, compared to the Kepler distribution. The initial distribution assumed as an ingredient of HB13 in the ELLISA simulation is also shown (dotted) and corresponds to the period distribution of the full binary population at zero-age (see Section 2.1). By contrast, the distribution shown for ELLISA corresponds only to the binaries that, at the selected age of the population, turn out to be eclipsing (based on the criterion described in Section 2.2). There are some clear differences between the ELLISA and Kepler period distributions, although the shape is similar overall. At the short-period end, there is a sharp drop off at ~ 0.1 d while in the Kepler distribution, which happens at a slightly lower period in ELLISA $\sim 0.02 - 0.03$ d. At the long-period end, the drop-off is much shallower in Kepler and while the ELLISA distribution falls-off rapidly at periods larger than ~ 10 d. This more notable difference is probably due to the criteria used to decide when a binary is eclipsing or not. Some of this differences also might stem from the choice of initial

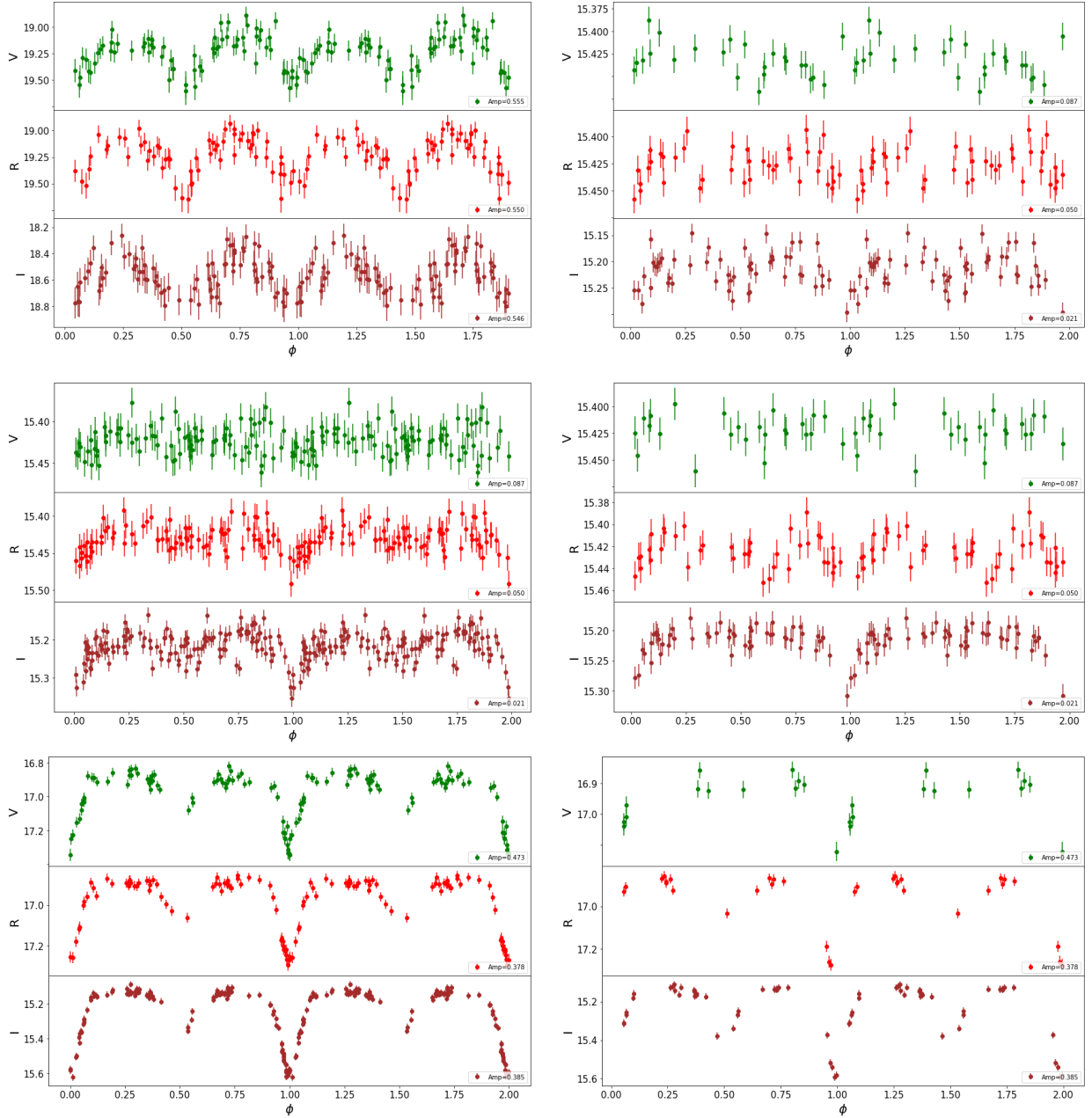


Figure 4. Simulated QUEST VRI light curves: EW system (upper panels), EB system (middle panels) and EA system (bottom panels) with very dense (left panels) and very sparse (right panels) time sampling .

period distribution made in HB13. In the future we plan to explore different initial assumptions for some of the zero-age orbital parameters and possible introduce distributions that consider joint dependencies (e.g. [Moe & Di Stefano 2017](#)). For the time being, since this modifications are beyond the scope of this work, we caution the reader that the use of ELLISA be better restricted to simulating eclipsing binaries with periods $\lesssim 15$ d.

3 THE SEARCH FOR ECLIPSING BINARIES IN THE QUEST LOW-LATITUDE CATALOGUE OF VARIABLE STARS

In what follows we identify candidate variables in the QUEST low-latitude survey and, over the sample of candidates, we conduct a period search using the available filters simultaneously and identifying possible spurious periods.

To characterise the completeness of the variable stars identification, we use ELLISA to generate a mock catalogue to mimic the time sampling and photometric errors of the QUEST survey. We search for candidate variables and de-

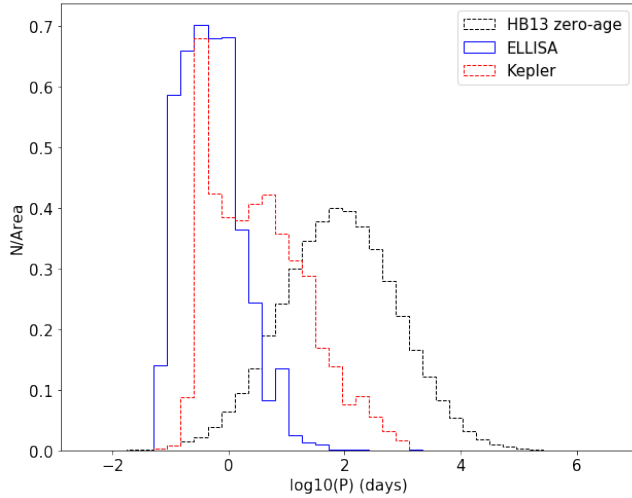


Figure 5. Period distribution resulting for a realization of a Thin Disc population of ELLISA eclipsing binaries (solid line), compared to the Kepler eclipsing binaries catalogue (Kirk et al. 2016) (dashed line). The initial period distribution assumed by HB13 (dotted line) for all binaries at zero-age is also shown for reference. All distributions shown are normalised to unit area.

termine the fraction of recovered variables using the same technique in terms of apparent magnitude and amplitude.

3.1 The QUEST low-latitude survey

In this work we make use of the QUEST variability survey at low galactic latitude from M12. This catalogue spans a total area of 476 deg² with 6,513,705 point sources and consists of multi-epoch observations in the VRI filters obtained fully with the Jürgen Stock Schmidt telescope and the QUEST-I camera (Baltay et al. 2002) at the National Astronomical Observatory in Llano del Hato, Mérida, Venezuela. The observations correspond to a low Galactic latitude zone in the range $-25^\circ \lesssim b \lesssim 30^\circ$ approximately in direction towards the Galactic anti-centre $190^\circ \leq l \leq 230^\circ$.

The time sampling of the survey is quite inhomogeneous as it comprises observations from many different projects with different scientific goals, and spans observations obtained between November 1998 and June 2006. Each star was typically observed once in any given night, with some exceptions of areas surveyed more than once (e.g. around McNeil’s nebula in Orion). The typical number of epochs per star is ~ 30 in V,R and ~ 25 I respectively, but these can range from ~ 10 up to ~ 120 –115 depending on the area of the sky (see Figure 5 in M12 and Figure 6 in Section 3.2).

The saturation magnitudes M_{sat} are 14.0 mag for V and R and 13.5 mag for I, the limiting magnitudes M_{lim} are 19.7 mag for V and R and 18.8 mag for I and the completeness magnitudes M_{com} are 18.5 mag for filters V and R and 18.0 mag for filter I. For full details of the survey we refer the reader to M12.

3.2 The ELLISA-QUEST Mock Light Curve Catalogue

Here we describe the catalogue of synthetic light curves produced with ELLISA to mimic QUEST, which is later used to fine-tune the variable star selection thresholds and period search parameters used in the search for eclipsing binaries.

First we randomly select $> 300,000$ of the stars (5%) out of the M12 QUEST catalogue, in order to use the time sampling of each one as an input for ELLISA. This way we can have a simulation with a time sampling in the VRI bands that is representative of the whole survey and that reproduces the different cadence and number of observations across the survey area. For the QUEST M12 survey, this is a particularly important point since the time sampling and number of observations per filter is very inhomogeneous across the survey.

The mock light curve catalogue was simulated within the saturation and completeness limits quoted in the previous section for the QUEST survey. Error versus magnitude curves were used as a function of the location in the survey footprint, computed by M12 subdividing the whole catalogue in stripes of 1h in right ascension by $0^\circ.55$ in declination, allowing to take into account the effect of the changing number of observations per object per filter on the photometric error in different survey regions. Figure 6 illustrates the number of observations per filter in a map in equatorial coordinates.

The ELLISA-QUEST Mock Light Curve Catalogue was produced using the simulator described in Section 2, assuming a Thin-Disc-like population. This is a reasonable assumption as the M12 QUEST survey is concentrated at low galactic latitudes ($|b| < 30^\circ$) where the population is expected to be dominated by the Galactic Thin Disc. In any case, at such old ages ($\gtrsim 8$ –9 Gyr), the overall binary properties change very little with age. So, including a Thick-Disc-like population would be equivalent to giving a slightly larger weight to the old Thin Disc population and should not produce very significant changes.

The synthetic light curve catalogue produced containing a total of 307,935 binaries, of which 206,313 are EA systems and 101,622 EB+EW systems. The period and V band amplitude distributions are shown in the upper and lower panels of Figure 7, respectively. As expected, EA systems dominate the distribution at large periods. It is interesting to note that, in the amplitude distribution, EB+EW systems dominate at large values (> 1 mag). This is due to the presence of EW systems composed of massive Main Sequence star pairs, in which stars have large radii ($> \text{few } R_\odot$), common in young populations present in our Disc-like mock population. These binaries are largely absent in old Thick-Disc-like or Halo-like populations (except, e.g., for cases that produce Blue Straggler stars).

The mock catalogue with VRI synthetic light curves is publicly available at the GitHub repository³.

In what follows we will use this synthetic or mock light curve catalogue to guide parameters used in the search for eclipsing binaries and to characterise the completeness of the samples at various stages of the identification process.

³ https://github.com/umbramortem/QUEST_EBs

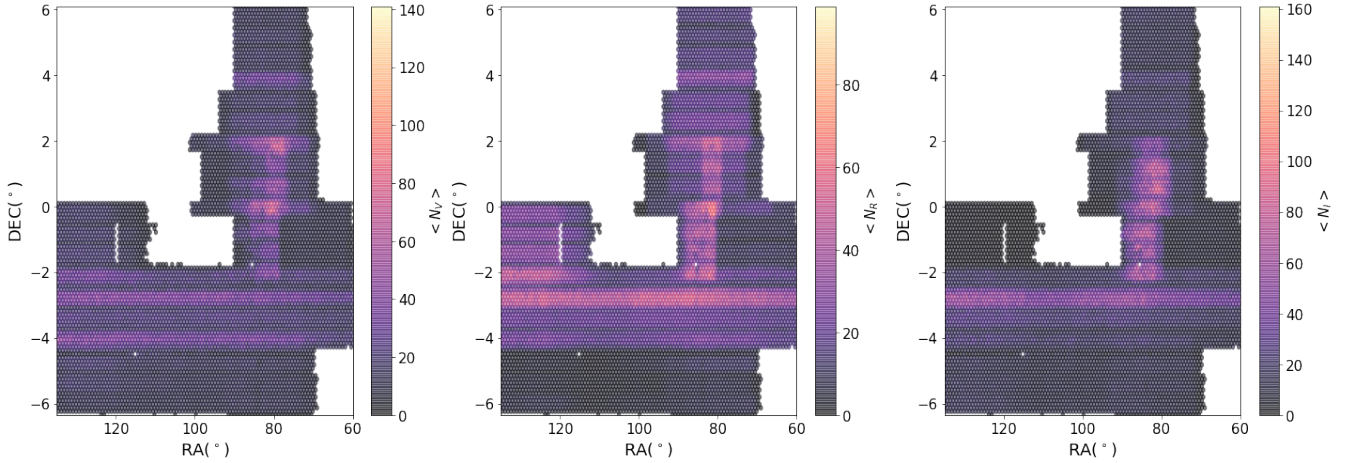


Figure 6. Spatial distribution of the number of observations for filters V (left), R (middle), I (right) of the mock catalogue, in equatorial coordinates. The colour scale in each panel indicates the mean number of observations for each filter for each star.

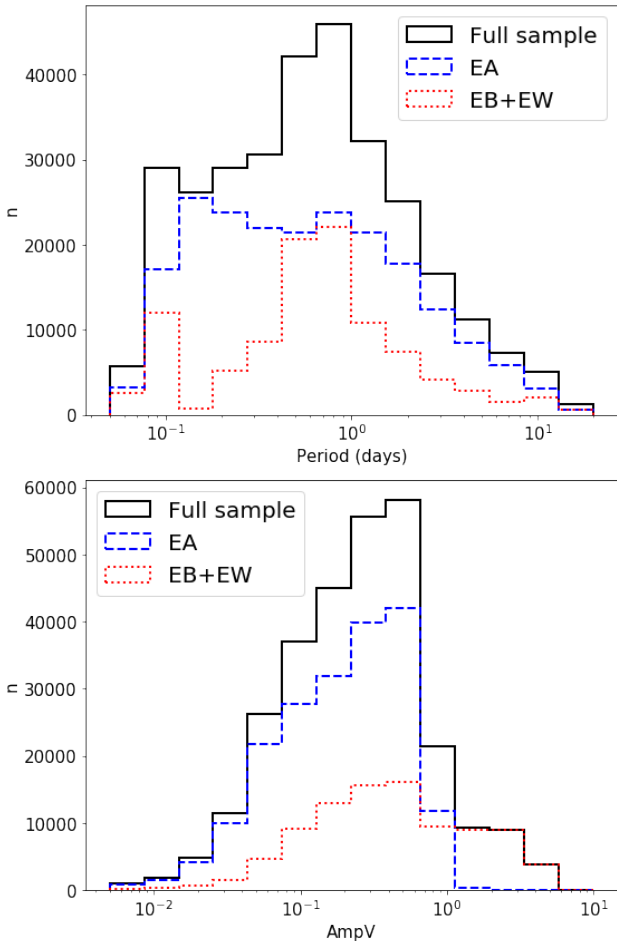


Figure 7. Period (upper panel) and V amplitude (lower panel) distribution of full sample (solid black line), EA systems (dashed blue line) and EB+EW systems (dotted red line) of the mock catalogue.

3.3 Variable star identification

The first step in the search for eclipsing binaries is to identify stars exhibiting photometric variability. To identify variable stars we used the M12 extension of the variability indices defined by Stetson (1996). These indices use the fact that the variability in two different photometric passbands must be positively correlated for most known types of variable stars. In the M12 catalogue, the three possible Stetson L indices L_{VR} , L_{VI} and L_{RI} are reported for each star.

Due to the inhomogeneous coverage of the survey, there are areas with very few observations in one or more filters, or even missing information in one filter altogether. Therefore, as in M12, we selected as variable stars those that meet the following criteria:

- $L_{VR} \geq 1$ or $L_{VI} \geq 1$ or $L_{RI} \geq 1$
- Observed amplitude ≥ 0.2 mag, at least for two filters
- $N_{obs} \geq 10$, at least for two filters

From the whole QUEST sample of 6,513,705 stars, using this criteria a total of 410,715 stars were selected as candidate variables. We also applied this methodology to the ELLISA-QUEST mock catalogue and 60,145 objects were selected as variable stars.

3.4 The period search

The search for eclipsing variables was conducted using the Lafler & Kinman (1965) method developed to identify light curve periods of variable stars. In this work we used the extension presented in M12 that allows the use of the multi-filter data in the survey. This method chooses as the best period the one that makes the light curve look smooth when period-folded. For the purposes of this work, we proceed following M12 but adapted the range of the periods search to a wider one considering that the stars studied by M12 are RR Lyrae which have a shorter period range than eclipsing binaries. The period range chosen was from 0.04 d to 15 d, searched with an initial resolution of 10^{-4} d, refining the

best 5 periods with a resolution of 10^{-7} d, and ending with the selection of the 3 best periods.

In addition to the period calculation, we computed the parameter Λ , a statistical significance parameter that describes how smooth the light curve is for a given trial period, compared to the median for all trial periods, in standard deviation units ($N\sigma$). M12 used a conservative threshold of $\Lambda = 4$ to search for RR Lyrae stars, i.e. stars for which a trial period was found to smooth the light curve at a 4σ statistical significance. After a visual inspection of a significant fraction of the sample, we observed that those light curves with values of Λ close to 4 were extremely noisy. Because of this, we selected a higher threshold and performed the visual inspection only for those curves with $\Lambda \geq 5$, which resulted in a sample consisting of 10,020 initial candidates.

3.4.1 Period aliases

Vivas et al. (2004) and M12 have shown that in the QUEST survey the period aliasing is frequent due to periodicities in the time sampling. Hence, we used the mock catalogue of eclipsing binaries to identify the most common period aliases affecting our survey.

According to Lafler & Kinman (1965), the spurious periods Π follow the relation

$$\frac{1}{\Pi} = \frac{k}{P} + \frac{1}{p} \quad (5)$$

with P the true period, k a rational number that produces the harmonics of P and p the external period present in the time sampling. M12 analysed the most frequent period aliases that affect the recovery of RR Lyrae stars in their survey. They found the most frequent one is the one-day alias and the less frequent aliases were the 1/3-day and 1/4-day aliases for RRab stars and for the RRc type the first harmonic of the true period and the 1/2-day alias. In this work we have repeated that analysis and summarise our results in Table 2. In addition to the common period aliases found in M12, observe the presence of half the period harmonic aliases with $k = \frac{1}{2}$, as well as another very important locus represented by the 1/20-day (1.5 h) alias. This period alias is interesting as it is probably due to the repeated observations obtained as part of the CIDA variability survey of Orion around the McNeil nebula (Briceño et al. 2004), which had precisely a 1.5 h cadence.

The most common aliases identified in this analysis were used in the visual inspection of the light curves during the search of eclipsing binaries in the real catalogue. Alias periods are reported wherever disambiguation was not possible.

3.5 The QUEST catalogue of Eclipsing binaries

The final identification of eclipsing binaries was made by visual inspection of the full sample of 10,020 initial candidates for which a statistically significant period ($\Lambda \geq 5$) was found. The light curves were period-folded with the three best periods found, and the five most common period aliases identified in Section 3.4.1 were also checked for the best period selected.

Finally, we obtained 1,125 eclipsing binaries consisting

Table 2. Frequency of occurrence of the different aliases or spurious periods present in the mock catalogue of eclipsing binaries

Type	k	p (d)	Frequency(%)
Correctly identified	1		14.3
Harmonics	$\frac{1}{2}$		2.79
	2		16.4
	$\frac{1}{4}$		0.57
	4		0.53
	$\frac{1}{5}$		0.4
	5		0.07
	$\frac{1}{20}$		0.37
	20		0.001
1-day alias	1	± 1	0.4
	2	± 1	1.4
$\frac{1}{2}$ -day alias	1	$\pm \frac{1}{2}$	0.1
2-day alias	1	± 2	0.4
$\frac{1}{3}$ -day alias	1	$\pm \frac{1}{3}$	0.12
3-day alias	1	± 3	0.3
$\frac{1}{4}$ -day alias	1	$\pm \frac{1}{4}$	0.1
4-day alias	1	± 4	0.17
$\frac{1}{5}$ -day alias	1	$\pm \frac{1}{5}$	0.03
5-day alias	1	± 5	0.12
$\frac{1}{20}$ -day alias	1	$\pm \frac{1}{20}$	0.01
20-day alias	1	± 20	0.07

of 179 EA, 60 EB and 886 EW systems corresponding to 16%, 5% and 79% of the catalogue respectively.

The main light curve parameters are summarised in Table 3 and VRI light curves are shown in Appendix A. The VRI time series data are available at a public GitHub repository⁴.

3.5.1 Cross-match with public catalogues of variable stars

We cross-matched our 1125 Eclipsing Binaries candidates with the ASAS-3 catalogue (Pojmanski 1997), the GCVS (Samus et al. 2009) and the Catalina Real-Time Transient Survey (CRTS) (Drake et al. 2014b) with a tolerance of 7 arcsec. We found no coincidences with ASAS-3, and found 384 and 12 matches with CRTS and GCVS respectively.

Out of the 384 matches with CRTS, shown in Table 5, 298 stars are classified as EW, 1 as EB and 25 as EA in both catalogues. Of the 60 matches left, 31 stars are classified as EW in the QUEST catalogue having different classifications in the CRTS catalogue, being 2 EB, 3 EA, 9 RS CVn, 1 RRab, 14 RRc, 1 RRd and 1 Hump (erratic light curve); 19 stars classified as EB in the QUEST catalogue are reported as EA (1) and EW(18) stars in CRTS; and 10 stars classified as EA in the QUEST catalogue and classified as 1 EA with unknown period, 1 EB and 8 EW stars respectively in the CRTS catalogue. It should be noticed that 12 of the CRTS periods resulting from the cross-match are found to be inexact based on the light curve inspection as indicated by Drake et al. (2014b). We found 180 stars having the same period we obtained in this work within a tolerance of 5%. These, as well as stars identified with a period alias are indicated in Table 5. Looking at the most common period aliases for the

⁴ https://github.com/umbramortem/QUEST_EBs

Table 3. Basic information and light curve parameters of the eclipsing binaries identified. (This table is published in its entirety as Supporting Information with the electronic version of the article. A portion is shown here for guidance regarding its form and content).

ID	RA (°)	DEC (°)	(N_V, N_R, N_I)	Period (d)	AmpV (mag)	AmpR (mag)	AmpI (mag)	Type	V (mag)	R (mag)	I (mag)
40430964	73.3967	1.21155	(23,24,26)	0.36275	0.48	0.50	0.45	EW	16.52 ± 0.02	16.04 ± 0.01	15.66 ± 0.01
40440270	73.5137	1.10068	(26,25,26)	0.62019	0.41	0.46	0.41	EB	14.85 ± 0.01	14.69 ± 0.00	14.52 ± 0.01
40451647	73.6484	1.19106	(19,25,25)	0.26241	0.62	0.62	0.64	EW	17.52 ± 0.04	17.12 ± 0.01	16.76 ± 0.02
40507509	74.3014	1.23649	(24,25,27)	0.43003	0.21	0.26	0.28	EW	16.56 ± 0.02	16.24 ± 0.01	15.95 ± 0.01

The Table columns are: the identification number ID, right ascension RA and declination DEC (J2000), the number of observations in the VRI bands, the light curve period, amplitude of variation in each band, type of eclipsing binary and mean magnitudes in each band with the corresponding photometric error.

matched stars, we found 9 stars were recovered at half the period, 3 at twice the period and 1 three times the period. We also found 20 alias of 1-day, 5 of 1/3-day, 11 of 1/2-day and 4 of 1/4-day.

Table 4 summarises the matches with GCVS. Out of the 12 matches, 4 stars don't have a computed period in GCVS and are classified there as one rapid irregular in a nebula (NN Ori), one rapid irregular (V1891 Ori), one red rapid irregular (V2678 Ori) and one UV Ceti (V0678 Ori). These stars were all classified in our catalogue as being EW.

Out of the 8 matches left, 6 were catalogued in GCVS as being RRc stars of which 1 is suspected to be alias of half the period (V0473 Hya), 2 alias of 1-day (V1867 Ori and V1845 Ori) and 3 alias of 1/2-day (V0497 Hya, V0485 Hya and V0944 Mon). These stars are kept in our final catalogue classified as EW type, since upon visual inspection the curves seem smooth and the amplitude of the eclipses similar for the different filters, as expected for EW binaries. Finally, the two stars left were classified in GCVS as a Delta Scuti with a suspected alias of 1 of 1/3-day (V2742 Ori), an a EW (V2769 Ori). These stars are classified in our catalogue as EWs. We retain their classifications as EW since the amplitudes for the three filters are very similar, although we caution that star 51082306 is near the faint limit of our survey ($V = 17.6$ at maximum light) and its light curve is noisy.

Our catalogue also overlaps partially with the van Eyken et al. (2011) eclipsing binaries catalogue from the Palomar Transient Factory (PTF) Orion Project. Out of their total of 82 binaries, we find 22 matching systems, with 16 of them classified as Close systems (C) which corresponds to EW+EB systems in our classification and 5 as Detached (D) which corresponds to our EA systems, in both catalogues, and 1 system classified in this work as EW and classified as EA system by van Eyken et al. (2011). We found 9 period matches, an alias of 1-day and 1 alias of half the period.

We also cross-matched our catalogue with the T Tauri star catalogue from Karim et al. (2016), since it is based on the QUEST low-galactic-latitude catalogue with additional observations made by the YETI project for some objects. We found 18 resulting matches, all classified in our catalogue as EW and as 2 Classical T Tauris (CTTS) and 16 weak-lined T Tauris (WTTS) in Karim et al. (2016). Data for these stars in Karim et al. (2016) catalogue are shown in Table 5, were the identified period aliases are also reported. These matching objects could be potential T Tauri stars in

binary systems. However, a more detailed analysis of the light curves would be warranted to confirm this since most are recovered here at twice the period, meaning that only one of the two variability causes is probably real. It is important to note, however, that the low fraction of matching objects on both catalogues, 8% of Karim et al.'s and <2% of ours, supports that a low degree of contamination or confusion is expected in either catalogue.

4 COMPLETENESS OF THE QUEST CATALOGUE OF ECLIPSING BINARIES

In order to analyse the completeness of the catalogue of eclipsing binaries produced, we used the procedure described in the previous sections to select variable stars and conduct the period search over the ELLISA-QUEST mock catalogue of eclipsing binary light curves. We considered 'recovered' all synthetic variables for which the accumulated phase shift α due to the period misidentification is less than 20%, $|\alpha| < 0.2$, where α is given by

$$\alpha = \frac{(P_{\text{recovered}} - P_{\text{true}})}{P_{\text{true}}} \frac{\Delta T}{P_{\text{true}}} \quad (6)$$

where ΔT is the average duration of the time series, weighted by the number of observations in each filter.

Figure 8 shows the resulting completeness as a function of the apparent V, R and I band magnitudes. The full sample of synthetic stars with recovered periods corresponds to the black circles. This is sub-divided into three sub-samples according to VRI band amplitudes: $0.2 \leq \text{Amp} \leq 0.5$ (yellow triangles), $0.5 \leq \text{Amp} \leq 1$ (red diamonds) and $\text{Amp} \geq 1$ (blue squares). Note that, in this and the following figures, the curves represent the completeness or recovery fraction within each sub-sample, so the sum of curves for the different sub-samples is *not equal* to the curve for the combined sample.

For the three ranges selected, the plot shows the completeness decreases monotonically for fainter objects. Also, the recovery is systematically larger for stars in the intermediate-amplitude range, which is to be expected. Lower amplitude stars are more difficult to identify as variables and their periods more difficult to recover, due to the noisier data. Higher amplitude stars, on the other hand, are mostly EA binaries with very abruptly varying light curves for which the Lafler & Kinman (1965) method is not optimal, and which are often miss-identified as non-variables,

Table 4. QUEST matches with the GCVS catalogue.

ID _{QUEST}	P_{QUEST} (d)	AmpI (mag)	Type _{QUEST}	ID _{GCVS}	P_{GCVS} (d)	AmpI (mag)	Type _{GCVS}	Comments (periods)
50727050	0.303348	0.442	EW	V1867 Ori	0.217985	0.5	RRC:	1-day alias
51082306	0.387926	0.424	EW	V2742 Ori	0.162376	0.30000114	DSCT:	1/3-day alias
80683482	1.291147	0.468	EW	V0497 Hya	0.391934	0.6000004	RRC	1/2-day alias
51556152	0.214918	0.614	EW	V2769 Ori	0.27872	...	EW	...
50130978	0.337271	0.408	EW	V1845 Ori	0.254789	0.40000057	RRC:	1-day alias
80312834	0.690166	0.406	EW	V0473 Hya	0.345091	0.5	RRC	k=2 harmonic
80010865	0.418573	0.25	EW	V0944 Mon	0.209273	0.29999924	RRC:	1/2-day alias
80494973	0.480576	0.408	EW	V0485 Hya	0.240283	0.3000002	RRC	1/2-day alias
50917935	0.474314	0.304	EW	V1891 Ori	...	0.42000008	IS	...
51000045	1.66799	0.327	EW	V2678 Ori	...	0.10999966	INSB	...
50765586	4.648128	0.365	EW	V0678 Ori	...	2.0	UVN	...
50969201	10.696515	0.331	EW	NN Ori	...	2.500001	INS	...

Table 5. QUEST matches with the CRTS catalogue. (This table is published in its entirety as Supporting Information with the electronic version of the article. A portion is shown here for guidance regarding its form and content)

ID _{QUEST}	P_{QUEST} (d)	AmpV (mag)	Type _{QUEST}	ID _{CRTS}	P_{CRTS} (d)	AmpV (mag)	Type _{CRTS}	Comments (periods)
40047541	0.263274	0.307	EW	J041329.6-031402	0.26327	0.21	EW	matches
40067341	0.310505	0.329	EA	J041810.3-024627	...	0.07	EA _{UP}	...
40083051	0.352228	0.328	EW	J042232.8-015739	0.352226	0.2	EW	matches
40141914	0.409572	0.523	EW	J043216.2-015942	0.29033	0.55	EW	1-day alias
40152097	0.267945	0.666	EW	J043338.3-015918	0.23621	0.38	EW	

Table 6. QUEST matches with the PTF catalogue ([van Eyken et al. 2011](#))

ID _{QUEST}	P_{QUEST} (d)	Type _{QUEST}	ID _{PTF}	P_{PTF} (d)	Type _{PTF} (periods)	Comments
50557720	0.313152	EW	6-3648	0.27066	C	...
50566490	0.540496	EW	6-5196	0.425248	C	...
50571345	0.328092	EW	6-4262	0.328103	C	matches
50747963	0.413978	EW	9-3480	0.342832	C	...
50775468	0.368418	EW	9-6659	0.310999	C	...
50812538	0.086737	EA	10-3009	2.234	D	...
50847483	0.468221	EW	10-2406	0.468237	C	matches
50876465	0.327801	EW	11-3313	0.281535	C	...
50879736	0.227755	EW	11-3778	0.227754	C	matches
50620504	0.504927	EW	7-750	0.402915	C	...
50707857	0.327595	EW	8-1414	0.281382	C	...
50863250	0.372698	EW	11-1051	0.372703	C	matches
50517261	0.852987	EA	0-8036	0.597359	D	...
50544270	0.26412	EW	0-8177	0.304414	C	...
50563048	0.273228	EW	0-5197	0.273236	C	matches
50820059	0.331189	EW	4-8796	0.397136	C	...
50830997	0.258346	EW	4-7558	0.258346	C	matches
50842277	0.264612	EW	4-9573	0.264623	C	matches
50545498	3.138798	EA	6-7525	1.569462	D	1-day alias
50569288	1.351627	EA	6-9087	1.351641	D	matches
50599532	2.071471	EW	7-7604	2.071092	D	matches
50602623	1.91986	EA	1-2659	0.960161	D	k=2 harmonic

given the difficulty to have well sampled eclipses. Also, note that in the two upper panels the mean completeness for the full sample is lower than for the three sub-samples. This is caused by the stars with data missing in one filter, or an observed amplitude < 0.2 mag, which are included in the

search; this is because in the criteria defined in Section 3.3 we only required two out of the three amplitudes to be larger than 0.2 mag.

Figure 9 shows the completeness as a function of period for each eclipsing binary type, for the full period range (top

Table 7. QUEST matches with the Karim et al. (2016) TTS catalogue.

ID _{QUEST}	P_{QUEST} (d)	Type _{QUEST}	ID _{KARIM}	P_{KARIM} (d)	Type _{KARIM}	Comments (periods)
40538170	1.793697	EW	259	0.9	WTTS	k=2 harmonic
50324694	2.318376	EW	330	0.54	WTTS	1/2-day alias
50493050	2.248062	EW	431	0.11	WTTS	k=20 harmonic
50607212	22.161642	EW	607	11.19	WTTS	k=2 harmonic
50611629	2.480004	EW	614	1.24	WTTS	k=2 harmonic
50627432	14.369345	EW	200	7.18	WTTS	k=2 harmonic
50643673	0.795061	EW	694	0.4	WTTS	k=2 harmonic
50650756	0.97408	EW	28	0.49	WTTS	1-day alias
50674665	9.984332	EW	218	5.06	WTTS	k=2 harmonic
50737943	3.084968	EW	968	2.82	WTTS	
50765586	4.648128	EW	1059	2.32	WTTS	k=2 harmonic
50765935	1.26327	EW	1056	0.63	WTTS	k=2 harmonic
50936079	1.279304	EW	129	0.64	CTTS	k=2 harmonic
50969201	10.696515	EW	1593	1.23	WTTS	1-day alias
51033757	1.054704	EW	154	0.53	WTTS	1-day alias
51052067	14.143456	EW	1803	7.07	WTTS	k=2 harmonic
51053661	9.496182	EW	1810	4.75	WTTS	k=2 harmonic
51293974	7.453762	EW	1951	3.73	CTTS	k=2 harmonic

panel) and zooming in on periods shorter than 1 d (bottom panel). EA binaries are shown with (blue) triangles, EB+EW binaries are shown with (red) diamonds, the combined sample is shown with (black) circles. The top panel shows that taken as a whole, the completeness is on average fairly low, just below 20% for all eclipsing types combined. In this full long-period range going up to 10 d periods, the EA's completeness is on average 20% which is similar to EB+EW's with an average completeness between $\sim 5\%$ and 35% . However, this trend is different in the bottom panel focused on periods shorter than 1 d. For this short periods, the EW+EB binaries are optimally recovered with completeness averaging $\sim 30\%$ for periods larger than ~ 0.3 d and, in contrast, EA's being recovered less than 5% on average. This confirms our expectation, based on results from the previous RR Lyrae surveys (Vivas et al. 2004, M12), that EW+EB can be effectively identified with QUEST. The average completeness found for the identification of EB+EW's might seem lower in comparison to the QUEST results for RR Lyrae stars of type *c*, but this is due to the much more stringent recovery criterion used here in comparison to Vivas et al. (2004) and M12.

Figure 10 also illustrates the dependence of the average completeness, independently of the binary type, for the full sample with $\text{AmpV} \geq 0.2$ mag (black circles) and in three amplitude ranges: short (yellow triangles), intermediate (red diamonds) and large (blue squares). These plots are representative of the behaviour for the R and I amplitudes as well, which are not shown for the sake of simplicity. This figure shows the dependence upon amplitude is not as strong as it is with type, shown in Figure 9. Binaries in the intermediate amplitude range are slightly better recovered on average, but this is simply a consequence of the correlation of amplitude with period and type, i.e. at a given period the strong dependence shown with type in Figure 9 dominates the average completeness trend more than the amplitude does. This very strong correlation with the eclipsing binary type has to do with the light curve shape and the survey's

time sampling: EW+EB's are easier to recover (<1 d) because of their smooth continuous light curves, as opposed to EA's sharper eclipses which are harder to sample. Therefore, the main factor that affects completeness is time sampling, rather than amplitude, which plays a secondary role.

Figure 11 shows the completeness as a function of the spatial distribution of the QUEST low latitude survey. The two panels show the similar overall variations, mainly influenced by the number of available observations as a function of RA-DEC. In the outermost parts of the survey the completeness is lower than that observed for zones with $-5^\circ \leq \text{DEC} \leq +5^\circ$. The latter, like the zone at $-2^\circ \leq \text{DEC} \leq 0^\circ$ and $60^\circ \leq \text{RA} \leq 80^\circ$, have the lowest number of observations of the survey and also has no observations in R and I (see Figure. 6). On the other hand for the zone between $-4^\circ \leq \text{DEC} \leq -2^\circ$ and $\text{RA} \geq 70^\circ$ the completeness is higher than for the previous zones. We observe that here the number of observations in the different filters is larger than the number for the previous region. Finally, the highest completeness belongs to the region between $1.5^\circ \leq \text{DEC} \leq 2^\circ$ and $70^\circ \leq \text{RA} \leq 90^\circ$ which has the larger number of observations for the three filters (typically > 100 observations per filter). We conclude that the completeness varies as a function of the number of observations available in each survey region, just as expected, since the fewer observations we have the worst sampled the curves will be, making the period recovery more difficult.

5 SUMMARY AND CONCLUSIONS

In this work we introduced ELLISA, a simulator that allows to generate a synthetic library of multi-filter light curves for a population of eclipsing binaries, from user-supplied time sampling and photometric errors. Mock eclipsing binary light curve catalogues produced with ELLISA can be used to test and optimise eclipsing binary searches in upcoming multi-epoch surveys, e.g. *Gaia*, PanSTARRS-1 or LSST, as well as to design observing strategies in future sur-

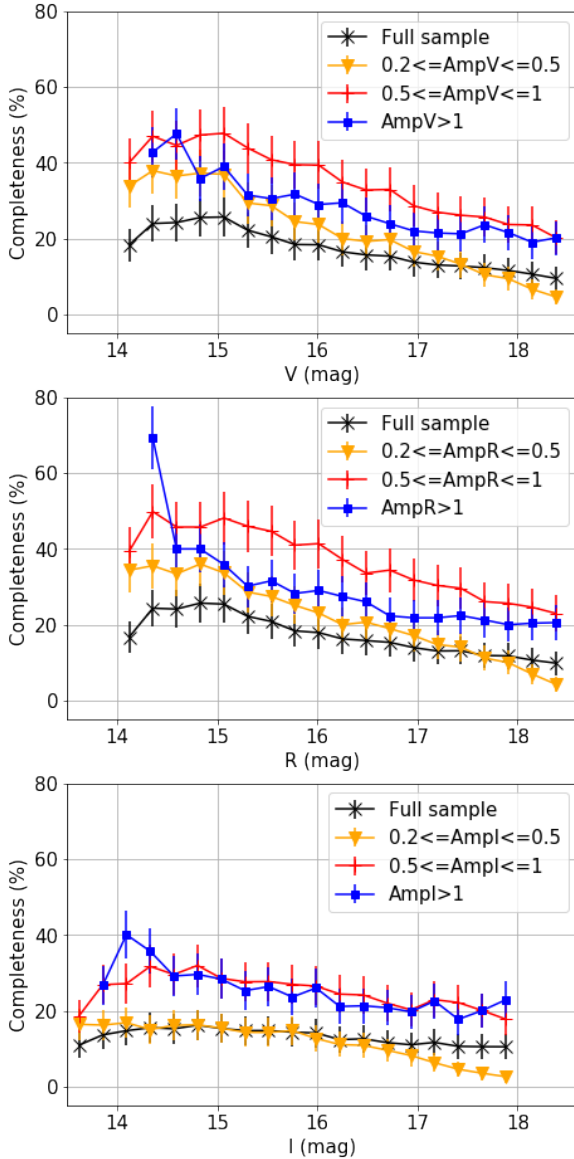


Figure 8. Completeness as a function of the V (top), R (centre) and I (bottom) magnitudes of the complete sample (black), stars with amplitudes between 0.2 and 0.5 magnitudes (orange), stars with amplitudes between 0.5 and 1 magnitudes (red) and stars with amplitudes larger than 1 magnitude (blue).

veys, with a realistic light curve ensemble. They can also be used to simulate the contamination due to eclipsing binaries in searches for other types of variables, such as RR Lyrae or SX Phoenicis/ δ Scuti stars. ELLISA is implemented in PYTHON and is publicly available in a GitHub repository⁵.

We have conducted an eclipsing binary search on the QUEST low latitude survey, and used ELLISA to guide and optimise search parameters for this particular survey, and to estimate the completeness of the resulting eclipsing binary catalogue as a function of binary type, apparent magnitude, period and amplitude. Our main results and conclusions are the following:

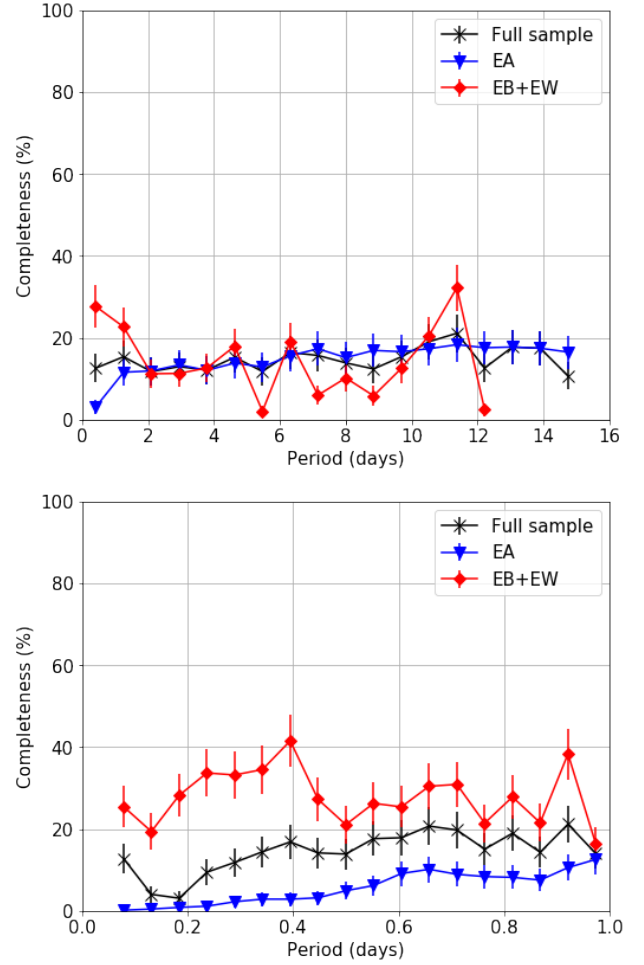


Figure 9. Completeness of the identification of eclipsing binaries in two period ranges: for the full period range explored (*upper panel*) and short periods < 1 d (*bottom panel*). In both panels the average completeness is shown for the full sample (black circles) and by type: EA (blue triangles) and EB+EW (red diamonds).

- We have identified 1,125 eclipsing binaries, out of which 707 are new discoveries, and consist of 139 EA (detached or Algol-type), 40 EB (semi-detached or β Lyrae-type) and 528 EW (contact or WUMa-type) corresponding respectively to 20%, 5% and 75% of the catalogue.

- The coordinates and light curve parameters of the eclipsing binaries identified are summarised in Table 3. The time series VRI data for the QUEST low latitude eclipsing binary catalogue is made publicly available at a GitHub repository⁶.

- EB+EW binaries are identified in QUEST with an average $\sim 30\%$ completeness in the period range 0.25–1 d

- EAs are identified at an average 15% completeness in the period range 2–10 d.

- Time sampling density is the primary factor affecting which types of eclipsing binary can be recovered and with what average completeness, while amplitude plays a secondary role.

⁵ <https://github.com/umbramortem/ELLISA>

⁶ https://github.com/umbramortem/QUEST_EBs

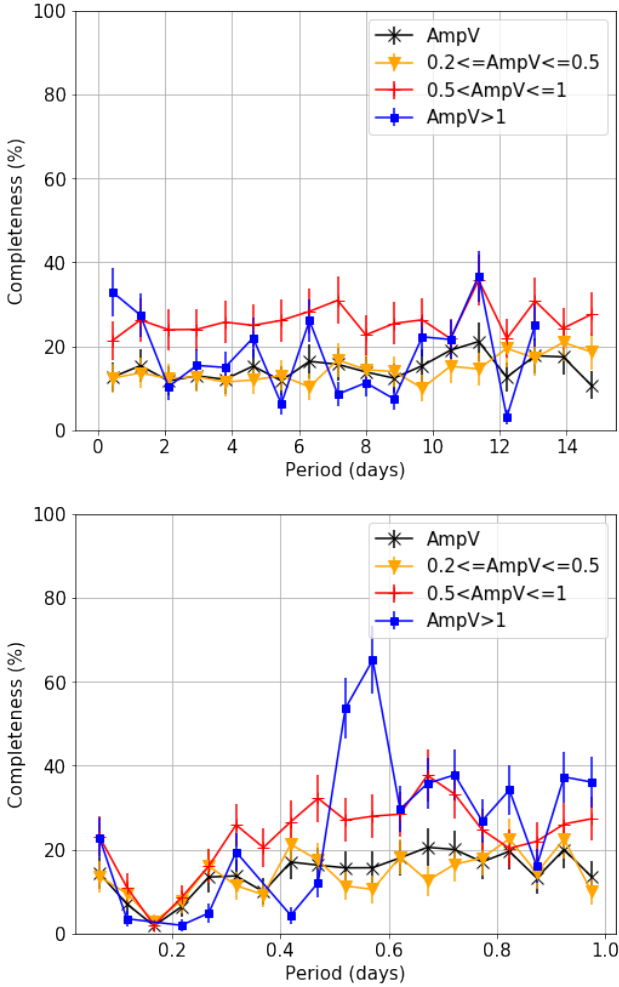


Figure 10. Completeness as a function of period for the full period range explored (*upper panel*) and short periods < 1 d (*bottom panel*), in three ranges of the V-band amplitude. The completeness for the full sample is shown with black circles, and for stars in three amplitude ranges: $0.2 \leq \text{AmpV}(\text{mag}) \leq 0.5$ (yellow triangles), $0.5 \leq \text{AmpV}(\text{mag}) \leq 1.0$ (red diamonds) and $\text{AmpV}(\text{mag}) \geq 1.0$ (blue squares). The behaviour shown by these plots is also representative of that for the R and I filters (not shown).

- This constitutes one of the few catalogues of eclipsing binaries reported to date with a complete characterisation of its selection function, provided as the completeness (recovery fraction) as a function of period, amplitude and apparent magnitude.

Being standard candles, EWs can be used to trace Galactic substructure and identify possible new overdensities, streams or dwarf satellites, or to infer Halo and Disc's density profiles, provided the selection function is known, as has been done in numerous previous studies with other standard candles such as RR Lyrae or Red Clump stars (Bovy et al. 2016; Mateu & Vivas 2018; Miceli et al. 2008). The EW catalogue presented here, particularly the high-completeness short-period sample (0.25–1 d), can therefore be used in any of these applications, given the provided char-

acterisation of the catalogue's selection function obtained with the ELLISA mock catalogues.

Acknowledgements The authors are glad to thank the referee, Andrej Prša, his valuable comments and recommendations which helped improve this work. B-CO would like to thank Kyle Conroy for his support with technical details in the implementation of PHOEBE.

REFERENCES

- Arenou F., 2011, in Docobo J. A., Tamazian V. S., Balega Y. Y., eds, American Institute of Physics Conference Series Vol. 1346, American Institute of Physics Conference Series. pp 107–121, doi:10.1063/1.3597593
- Baker M., Willman B., 2015, *AJ*, **150**, 160
- Baltay C., et al., 2002, *PASP*, **114**, 780
- Bovy J., Rix H.-W., Schlafly E. F., Nidever D. L., Holtzman J. A., Shetrone M., Beers T. C., 2016, *ApJ*, **823**, 30
- Briceño C., et al., 2004, *ApJ*, **606**, L123
- Brown W. R., Beers T. C., Wilhelm R., Allende Prieto C., Geller M. J., Kenyon S. J., Kurtz M. J., 2008, *AJ*, **135**, 564
- Chabrier G., 2003, *PASP*, **115**, 763
- Cohen J. G., Sesar B., Bahnhölzer S., He K., Kulkarni S. R., Prince T. A., Bellm E., Laher R. R., 2017, *ApJ*, **849**, 150
- Drake A. J., et al., 2013, *ApJ*, **763**, 32
- Drake A., et al., 2014a, *ApJ*, **213**, 9
- Drake A. J., et al., 2014b, *ApJS*, **213**, 9
- Duquenois A., Mayor M., 1991, *A&A*, **248**, 485
- Eggleton P., 2006, *Evolutionary Processes in Binary and Multiple Stars*
- Etzel P. B., 1981, in Carling E. B., Kopal Z., eds, *Photometric and Spectroscopic Binary Systems*. p. 111
- Gaia Collaboration et al., 2017, *A&A*, **601**, A19
- Green G. M., et al., 2015, *ApJ*, **810**, 25
- Han Z., Podsiadlowski P., Maxted P. F. L., Marsh T. R., Ivanova N., 2002, *MNRAS*, **336**, 449
- Hernández-Pérez F., Bruzual G., 2013, *MNRAS*, **431**, 2612
- Hurley J. R., Tout C. A., Pols O. R., 2002, *MNRAS*, **329**, 897
- Ivezić Ž., 2010, *Highlights of Astronomy*, **15**, 817
- Kaiser N., et al., 2010, in *Ground-based and Airborne Telescopes III*. p. 77330E, doi:10.1117/12.859188
- Karim M. T., et al., 2016, *AJ*, **152**, 198
- Keller S. C., Murphy S., Prior S., Costa G. D., Schmidt B., 2008, *ApJ*, **678**, 851
- Kinman T. D., Brown W. R., 2010, *The Astronomical Journal*, **139**, 2014
- Kirk B., et al., 2016, *AJ*, **151**, 68
- Lada C. J., 2006, *ApJ*, **640**, L63
- Lafler J., Kinman T. D., 1965, *ApJS*, **11**, 216
- Luck R. E., Kovtyukh V. V., Andrievsky S. M., 2006, *AJ*, **132**, 902
- Mateu C., Vivas A. K., 2018, arXiv, 1711.03967
- Mateu C., Vivas A. K., Downes J. J., Briceño C., Zinn R., Cruz-Diaz G., 2012, *MNRAS*, **427**, 3374
- Miceli A., et al., 2008, *The Astrophysical Journal*, **678**, 865
- Moe M., Di Stefano R., 2017, *ApJS*, **230**, 15
- Pojmanski G., 1997, *Acta Astron.*, **47**, 467
- Prša A., Zwitter T., 2005, *ApJ*, **628**, 426
- Prša A., Pepper J., Stassun K. G., 2011, *AJ*, **142**, 52
- Prša A., Zwitter T., 2005, *ApJ*, **628**, 426
- Reggiani M., Meyer M. R., 2013, *A&A*, **553**, A124
- Reggiani M., Robberto M., Da Rio N., Meyer M. R., Soderblom D. R., Ricci L., 2011, *A&A*, **534**, A83
- Robin A. C., et al., 2012, *A&A*, **543**, A100
- Rucinski S. M., 1994, *PASP*, **106**, 462

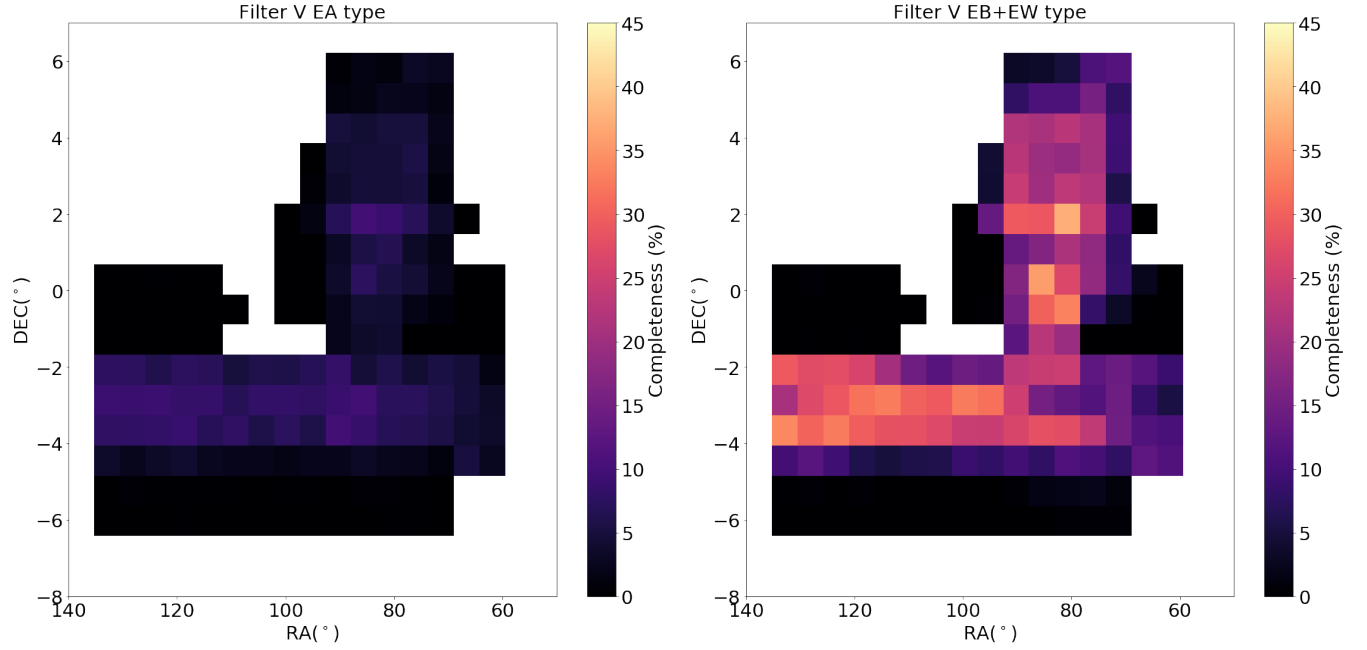


Figure 11. Spatial distribution of the average completeness in the recovery of eclipsing binaries (*left*:EA, *right*:EB+EW), in equatorial coordinates. Areas shown in black with null completeness correspond to survey areas with less than 10 epochs per filter on average (see 6).

- Rucinski S. M., 1996, in Milone E. F., Mermilliod J.-C., eds, *Astronomical Society of the Pacific Conference Series Vol. 90, The Origins, Evolution, and Destinies of Binary Stars in Clusters*. p. 270 ([arXiv:astro-ph/9508043](#))
- Rucinski S. M., 2004, *New Astron. Rev.*, **48**, 703
- Rucinski S. M., Duerbeck H. W., 1997, in Bonnet R. M., et al., eds, *ESA Special Publication Vol. 402, Hipparcos - Venice '97*. pp 457–460
- Sale S. E., et al., 2014, *MNRAS*, **443**, 2907
- Samus N. N., Durlevich O. V., et al. 2009, *VizieR Online Data Catalog*, **1**
- Sesar B., et al., 2010a, *ApJ*, **708**, 717
- Sesar B., Vivas A. K., Duffau S., Ivezić Ž., 2010b, *ApJ*, **717**, 133
- Sesar B., et al., 2017, *AJ*, **153**, 204
- Smith R. M., et al., 2014, in *Ground-based and Airborne Instrumentation for Astronomy V*. p. 914779, [doi:10.1117/12.2070014](#)
- Stetson P. B., 1996, *PASP*, **108**, 851
- Torrealba G., et al., 2015, *MNRAS*, **446**, 2251
- Vivas A. K., Zinn R., 2006, *AJ*, **132**, 714
- Vivas A. K., Zinn R., Abad C., Andrews P., Bailyn C., Baltay C., Bongiovanni A., et. al C. B., 2004, *The Astronomical Journal*, **127**, 1158
- Westera P., Lejeune T., Buser R., Cuisinier F., Bruzual G., 2002, *A&A*, **381**, 524
- Wichmann R., 2011, *Nightfall: Animated Views of Eclipsing Binary Stars*, *Astrophysics Source Code Library* (ascl:1106.016)
- Wilson R. E., Devinney E. J., 1971, *ApJ*, **166**, 605
- van Eyken J. C., et al., 2011, *AJ*, **142**, 60

APPENDIX A: ECLIPSING BINARY LIGHT CURVES

The catalogue of V, R and I period-folded light curves for all eclipsing binaries found in the survey is shown in Figure A1.

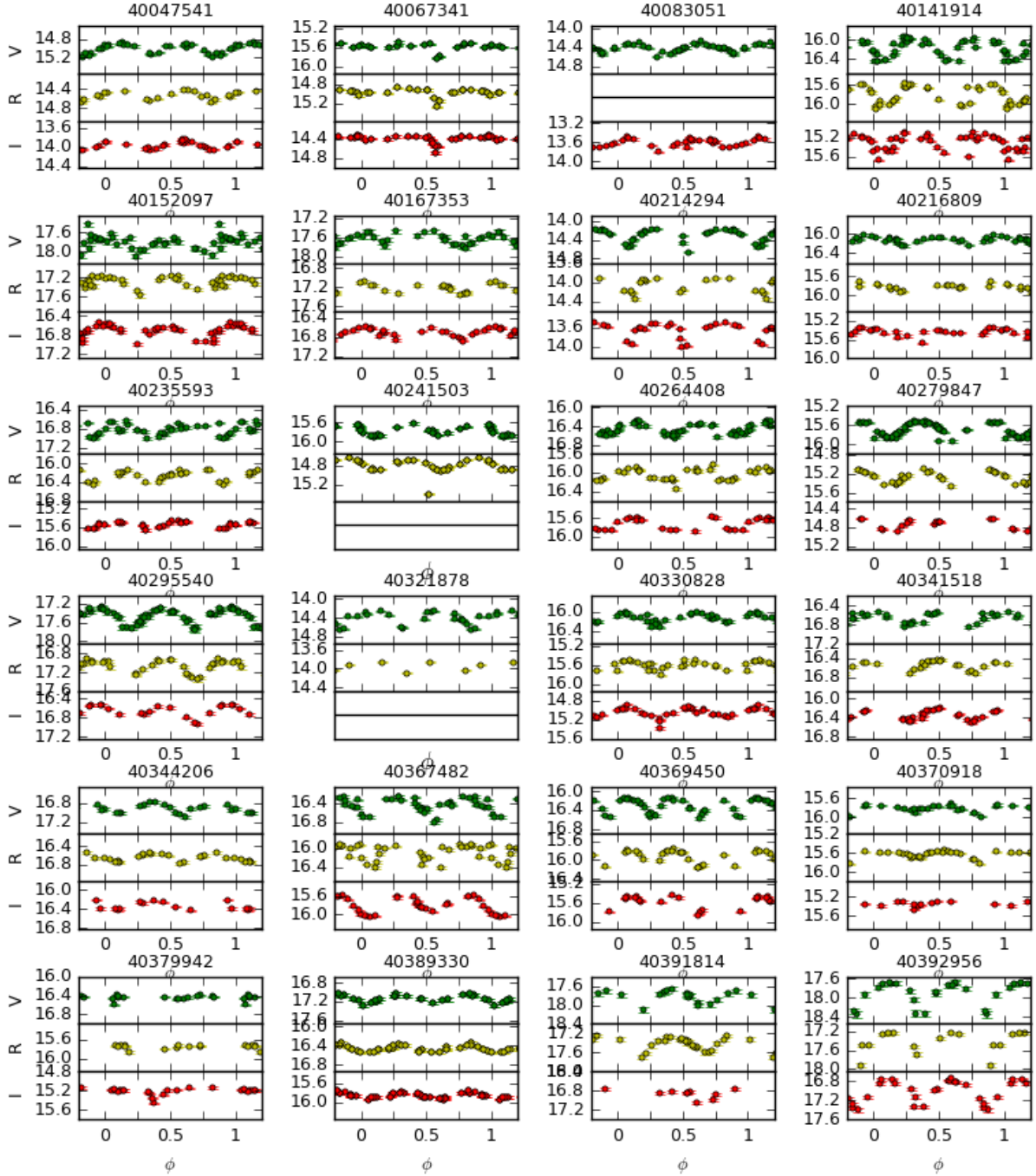


Figure A1. Light curves of survey eclipsing binaries. (This table is published in its entirety as Supporting Information with the electronic version of the article. A portion is shown here for guidance regarding its form and content.)